National Park Service
U.S. Department of the Interior

Natural Resource Stewardship and Science

Monitoring of Retrogressive Thaw Slumps in the Arctic Network, 2012

Natural Resource Data Series NPS/ARCN/NRDS—2013/591

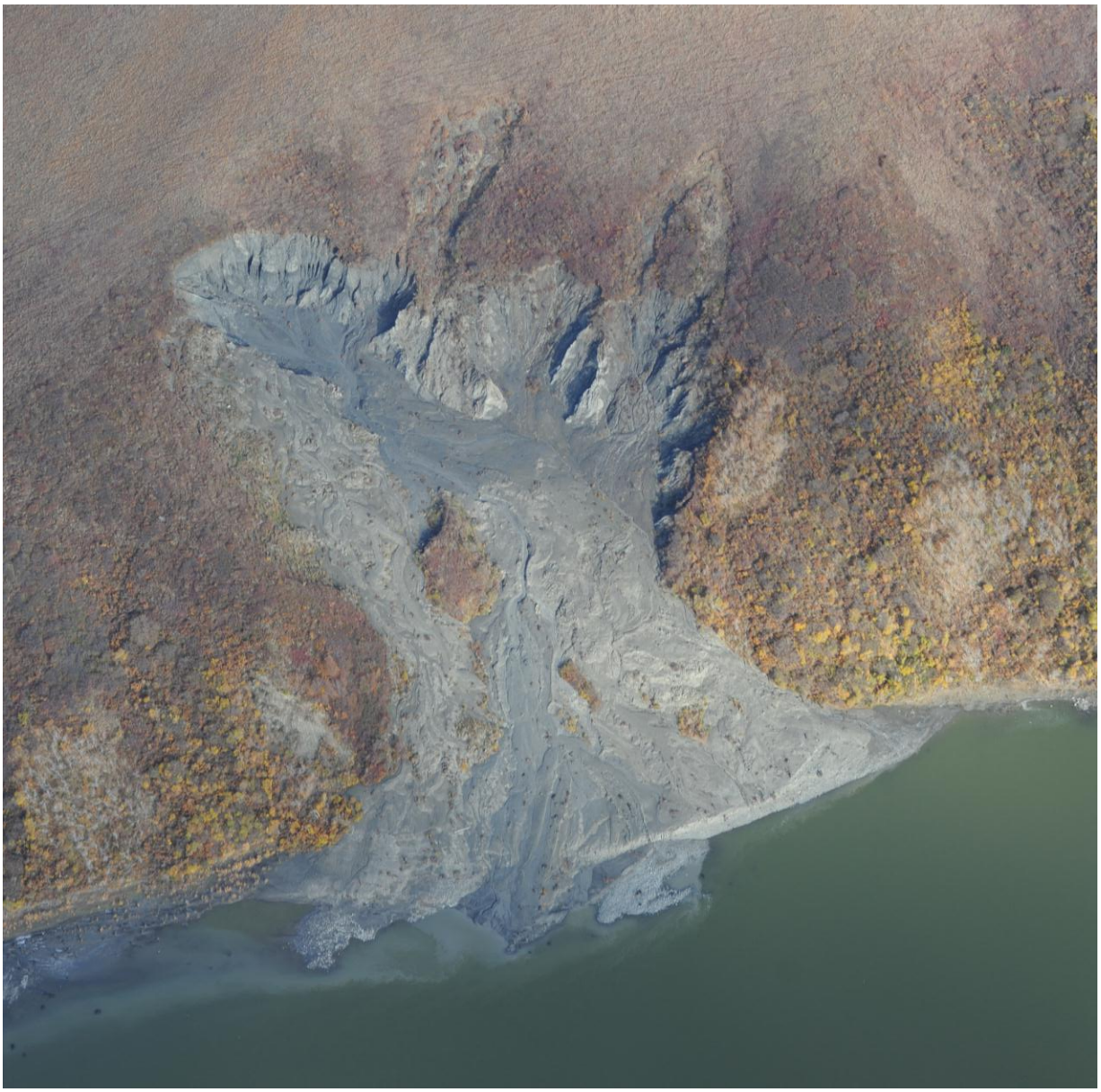

ON THE COVER

A large retrogressive thaw slump on the Noatak River in the Noatak National Preserve, Alaska. The distance from the top of the slump to the river was about 300 m at the time of this photo in 2012. This large and very active slump had a main scarp about 15 m high that migrated uphill 15 to 30 m between 2011 and 2012. This resulted in subsidence of about 50,000 m^3 in the upper part of the slump, balanced in part by a gain of about 10,000 m^3 on the slump floor below. The missing volume, which consisted of both sediment and water from melting of ground ice, was shed into the adjacent Noatak River.

Monitoring of Retrogressive Thaw Slumps in the Arctic Network, 2012

Natural Resource Data Series NPS/ARCN/NRDS—2013/591

David K. Swanson

National Park Service
4175 Geist Rd
Fairbanks, AK 99708

December 2013

U.S. Department of the Interior
National Park Service
Natural Resource Stewardship and Science
Fort Collins, Colorado

The National Park Service, Natural Resource Stewardship and Science office in Fort Collins, Colorado, publishes a range of reports that address natural resource topics. These reports are of interest and applicability to a broad audience in the National Park Service and others in natural resource management, including scientists, conservation and environmental constituencies, and the public.

The Natural Resource Data Series is intended for the timely release of basic data sets and data summaries. Care has been taken to assure accuracy of raw data values, but a thorough analysis and interpretation of the data has not been completed. Consequently, the initial analyses of data in this report are provisional and subject to change.

All manuscripts in the series receive the appropriate level of peer review to ensure that the information is scientifically credible, technically accurate, appropriately written for the intended audience, and designed and published in a professional manner.

Data in this report were collected and analyzed using methods based on established, peer-reviewed protocols and were analyzed and interpreted within the guidelines of the protocols.

Views, statements, findings, conclusions, recommendations, and data in this report do not necessarily reflect views and policies of the National Park Service, U.S. Department of the Interior. Mention of trade names or commercial products does not constitute endorsement or recommendation for use by the U.S. Government.

This report is available in digital format from the National Park Service, Arctic Inventory and Monitoring Network (http://science.nature.nps.gov/imn/units/arcn) and the Natural Resource Publications Management website (http://www.nature.nps.gov/publications/nrpm/). To receive this report in a format optimized for screen readers, please email irma@nps.gov.

Please cite this publication as:

Swanson, D. K. 2013. Monitoring of retrogressive thaw slumps in the Arctic Network, 2012. Natural Resource Data Series NPS/ARCN/NRDS—2013/591. National Park Service, Fort Collins, Colorado.

NPS 953/123090, December 2013

Contents

Figures

Page

Figures (continued)

Page

Tables

Page

Abstract

Retrogressive thaw slumps (RTS) are caused by thaw of massive ground ice on slopes and combine subsidence, mass movement, and water erosion. They can expose several hectares of bare soil that is susceptible to erosion into nearby water bodies. In the summers of 2010, 2011, and 2012, oblique aerial photographs of RTS in Noatak National Preserve (NOAT) and Gates of the Arctic National Park and Preserve (GAAR) were taken with a hand-held, 35-mm digital camera. These photographs were used to create high-resolution three-dimensional (3-D) topographic models. We also measured the slump areas on 2007-2008 high-resolution satellite images. The current report documents changes in 19 slumps for which we had ground surveys (for accurate scaling of the 3-D models) and photographs from multiple years including 2012.

Many of the slumps continued to grow rapidly from 2011 to 2012. The most rapid rates of main scarp retreat in 2011-12, after correction for the varying length of time between samples, were about 30 m per year at several slumps.

In nearly all cases growth rates were lower in 2011-12 than in 2010-2011 as reflected in rates of scarp migration, area growth, and subsidence volume. These declines in growth rate were usually accompanied by a decrease in main scarp steepness, and less exposure of massive ice in the scarp. The sum of thaw degree-days available to drive slump growth between our 2011and 2012 sample dates was less than what was available between our 2010 and 2011 sample dates. Thus these declines in slump growth rates were apparently due to factors internal to the slumps, such as escarpments migrating to areas with lower slopes or less ground ice.

Comparison of slump areas in 2010-12 with areas measured from high-resolution satellite images in 2007-2008 shows that slump growth rates were fairly constant 2007-2012 in most of the slumps, except those that showed the greatest recent growth slowdown. Extrapolation of the growth rates back in time from the earliest interval available (usually 2008 to 2010) suggests that all of these slumps initiated in the late 1990s and early 2000s.

The most active slump overall (NOAT265) lost nearly 50,000 m^3 of material in the vicinity of the main scarp, while less than a quarter of this volume accumulated in the lower part of the slump. The missing volume consisted of sediment and water that was shed into the adjacent Noatak River.

Acknowledgments

Thanks to the following people for their contribution to this monitoring study: Curtis Cebulski, Stan Hermens, and Quentin Slade (pilots); Ken Hill and Cody Priest (fieldwork); Tara Whitesell (logistical support and helicopter management); and Andrew Balser (slump locations and helpful discussions).

Introduction

Retrogressive thaw slumps (RTS) are dramatic features of the arctic landscape caused by thaw of permafrost. They occur where a cut-bank in ice-rich permafrost advances into undisturbed ground as material thaws in the steep bank, falls or slides onto the adjacent more gentle slope, and then is transported away by viscous flow or water erosion (Burn and Lewkowicz 1990). The advancing cut-bank, referred to here as the "main scarp" in keeping with standard landslide terminology (Beltran et al. 1993), is typically 2 to 10 m high, though it may reach 35 m (Crosby 2009). RTS often begin as escarpments produced by coastal, lakeshore, or fluvial erosion and then advance away from the shore by thaw and slumping. Very ice-rich material of substantial thickness (e.g., several meters) and lateral extent is needed to produce a RTS (Lacelle et al. 2010).

Because RTS are large erosion features that often occur near water bodies, they can affect water quality. Suspended sediment, ions in solution, and pH have been shown to be higher below RTS and other thermokarst erosion features (Bowden et al. 2008, Crosby 2009, Kokelj et al. 2005). Ions that increase include nutrient species such as potassium, phosphate, sulfate, ammonium, and nitrate, as well as other common soil base cations such as calcium, magnesium, and sodium.

While localized thaw and refreezing of permafrost occurs under a stable cold arctic climate, climate change has been cited as a cause of increased thaw of permafrost since 1982 in Alaska (Jorgenson et al. 2006). Concerns about the future state of permafrost led the National Park Service Arctic Inventory and Monitoring Network (ARCN, the five NPS units in northern and western Alaska) to include permafrost as a monitoring "vital sign" (Lawler et al. 2009). Thaw-related slumping and associated soil erosion may have increased in ARCN in recent years (Balser et al. 2007), and the activity of RTS in some areas of Canada has increased in recent decades (Lantuit and Pollard 2008, Lantz and Kokelj 2008).

In 2010 ARCN initiated a monitoring program for RTS (Swanson and Hill 2010). High-resolution three-dimensional (3-D) models of selected slumps were produced from oblique 35-mm aerial photographs together with surveyed ground control. Most of the slumps imaged in 2010 were re-photographed in 2011 and additional ground control was obtained where it was lacking in 2010, allowing me to document rates of change (Swanson 2012a). In 2012 most of the slumps were photographed again. The present report uses the photographs and survey data from 2010, 2011, and 2012, plus high-resolution satellite imagery from 2007-2008 to document the growth of these RTS.

Methods

Study Area and Site Selection

RTS were selected from mapped permafrost-related erosion features in ARCN (Swanson 2012, and unpublished data for Gates of the Arctic National Park and Preserve) and previous work by Balser et al. (2007). RTS were selected for intensive photographic monitoring based on 1) size, 2) potential for siltation of adjacent water bodies, 3) potential for encroachment on archeological sites, 4) visual impact, and 5) proximity to other slumps for economy of access (Fig. 1, Table 1).

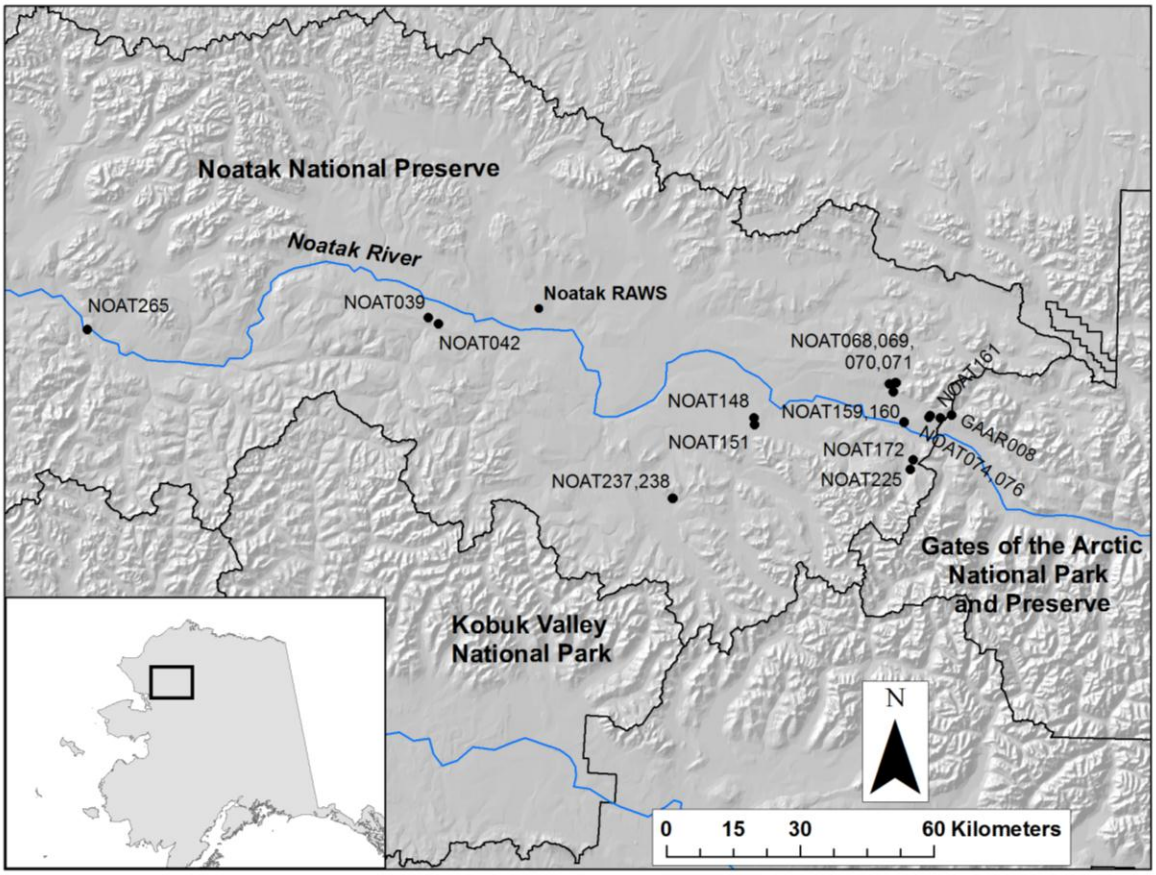

Figure 1. Locations of the retrogressive thaw slumps described in this report. A comprehensive list of all slumps with monitoring data is in Table 1.

All of the study RTS are within the zone of continuous permafrost (Jorgenson et al. 2008). Vegetation in NOAT is dominantly arctic tundra, with trees occurring at low elevations and mainly in the western part of the Preserve; of the slumps discussed in this report, only NOAT265 has trees on the adjacent slopes: balsam poplar (*Populus balsamifera*) and a few hybrid birch (*Betula nana* X *B. neoalaskana* hybrids.). Climate data from the Noatak RAWS shows a January mean temperature of -25.3 °C, July mean of 13.3 °C, and annual mean of -7.9 °C (WRCC 2011; for the period 1990-2011 with occasional missing values, mainly in the winter). This station is in the east-central part of the Preserve, in an area of tundra vegetation (Fig. 1).

Most of the RTS in this study were in late Pleistocene glacial deposits and had basal glacial ice exposed in the main scarp (Swanson and Hill 2010, Swanson 2012a). Melting of this laterally extensive massive ice drives the growth of these slumps. A few of the slumps were on older surfaces, where late Pleistocene eolian deposits with ice wedges overlie the till and glacial ice. For more information on the settings, scarp morphologies, and growth mechanism of these slumps, see Swanson and Hill (2010) and Swanson (2012a).

All of the slumps photographed in 2012 were previously photographed and surveyed to establish scale in 2010 or 2011 or both. Fieldwork in 2012 consisted solely of aerial photographs, with scale transferred to the 2012 photos from surveys completed in the previous years.

Table 1. Retrogressive thaw slumps monitored by ARCN, 2010-2012

Slump identifier	Longitude, deg-min W (NAD83)	Latitude, deg-min N (NAD83)	Fieldwork[1]			Analyzed in this report[2]
			2010	2011	2012	
GAAR008	156° 29.17’	67° 54.04’	s	s	p	√
GAAR010	154° 40.81’	68° 22.99’	s	-	-	
NOAT004	159° 14.65’	68° 04.22’	p	-	p	
NOAT037	161° 52.40’	67° 59.17’	-	s	-	
NOAT039	159° 17.48’	68° 02.15’	s	-	p	√
NOAT042	159° 14.08’	68° 01.43.’	s	-	p	√
NOAT068	156° 47.30’	67° 57.66’	s	p	p	√
NOAT069	156° 47.56’	67° 57.64’	s	p	p	√
NOAT070	156° 49.42’	67° 57.50’	s	p	p	√
NOAT071	156° 48.02’	67° 56.56’	s	-	p	√
NOAT072	156° 48.40’	67° 56.62’	p	-	p	
NOAT073	156° 49.14’	67° 56.85’	p	-	p	
NOAT074	156° 36.03’	67° 53.87.’	p	s	p	√
NOAT076	156° 36.27’	67° 53.66’	p	s	p	√
NOAT148	157° 31.94’	67° 52.61’	s	p	p	√
NOAT151	157° 31.60’	67° 51.77’	s	s	p	√
NOAT159	156° 44.15’	67° 52.98’	p	s	p	√
NOAT160	156° 44.12’	67° 52.87’	p	s	p	√
NOAT161	156° 32.86’	67° 53.61’	s	p	p	√
NOAT172	156° 40.90’	67° 48.39’	s	p	p	√
NOAT225	156° 41.59’	67° 47.25’	s	-	p	√
NOAT237	157° 56.12’	67° 42.30’	p	s	p	√
NOAT238	157° 56.16’	67° 42.24’	p	s	p	√
NOAT247	157° 51.10’	67° 40.18’	s	p	-	
NOAT248	157° 51.17’	67° 40.24’	s	p	-	
NOAT265	161° 05.06’	67° 56.85’	-	s	p	√

[1]”s” – ground control survey and photography; “p” – photography only.

[2]Slumps with a check (√) are shown in Fig. 1 and are described in the Results section of this report.

Aerial Photography

In 2012 aerial photographs were taken through the window of a de Havilland DHC-2 Beaver aircraft using a Nikon D700 camera, which has a "full-frame" (35-mm) sensor, and a 50 mm lens. The photos had oblique orientation (48° to 64° from vertical) and in most cases the aircraft was about 200 to 350 m from the middle of the target (Table 2). Photos were shot on several linear passes over the RTS, and the pass with the best coverage was chosen for model construction. Consecutive photos overlap to provide stereo coverage of the entire slump and adjacent areas; stereo coverage is needed to produce 3-D models. Photographs in 2010 and 2011 were taken out the door of a helicopter but had similar properties.

Table 2. Camera parameters summary for 2012 photos

Slump identifier	Pass	Average distance to target, m	Mean camera view angle ω, ° from vertical	Base:height ratio[2]
GAAR008	2012A	281	49	0.12
NOAT039	2012D	304	64	0.13
NOAT042	2012A	345	54	0.10
NOAT068	2012C	208	49	0.14
NOAT069	2013B	ND[1]	ND	0.14
NOAT070	2012C	343	56	0.09
NOAT071	2012A	ND	ND	0.13
NOAT074	2012A	196	52	0.14
NOAT076	2012B	192	48	0.14
NOAT148	2012A	272	48	0.11
NOAT151	2012B	247	57	0.14
NOAT159	2012A	279	61	0.10
NOAT160	2012A	314	63	0.10
NOAT161	2012A	340	53	0.09
NOAT172	2012C	273	49	0.13
NOAT225	2012A	463	62	0.11
NOAT237 & NOAT238	2012B	186	59	0.11
NOAT265	2012B	362	58	0.10

[1]ND – no data. Models for these slumps were not scaled and oriented with ground control (see the section "2-D Analysis" below) and thus have no distance or camera angle data; the base:height ratio can still be computed from relative units.

[2]Base:height ratio – the ratio between the distance traveled between photos and the distance to target.

3-D Model Construction

Three-dimensional models of the RTS were constructed from the oblique aerial photographs using Topcon Image Master software (www.topconpositioning.com). Each 3-D model presented here was constructed from multiple overlapping photos taken during a single flight pass. The size and

orientation of the 2012 models were obtained using locations of landmarks on models made in 2010 or 2011 years when a ground survey was completed (Table 1).

The procedure used in previous years for creating the models with ground control was as follows (Swanson and Hill 2010). Aerial markers were placed around the slump, and the distances separating them (both horizontal and vertical) were determined with a total station. Common points (i.e. natural features) identifiable on pairs of adjacent photos (known as "pass points") and the aerial markers with known coordinates (ground control points) were located on all of the photos. Image Master used these points to determine the location and orientation of the camera when each photo was taken, and to compute the locations of the pass points (in units of meters relative to the survey instrument location). The computation of camera and pass point locations was by bundle adjustment, which means that all photos, pass points, and ground control points were used simultaneously to compute the optimal solution.

After bundle adjustment, a 3-D surface of each slump was constructed in Image Master, by automated location of numerous common points on all the photographs. These points were spaced approximately 2 m apart.

For most slumps at least 10 pass points (typically rocks or small clumps of vegetation) from the surveyed year (2010 or 2011) were then located on 2012 photos, and their coordinates (as computed by bundle adjustment in the 2010 or 2011 model) were imported into the 2012 model as "tie points" with known absolute coordinates. Tie points can be difficult to locate on photos from different years taken from different perspectives. To make this process easier, I used the ArcMap Georeferencing Tools as described in Swanson (2012a). Then the 2012 models were created by the same method as the earlier models with ground survey, except I substituted these "tie points" for the surveyed ground control points. As a result the2012 models were co-registered with the model from the survey year.

Accuracy parameters for the models are given in Table 3. Model NOAT042 stands out with few control points and higher error; this was due to the difficulty in finding landmarks in the tall brush that surrounds this slump. In general these accuracy parameters are satisfactory (less than 1 m mean error), but registration of models from photographs taken two years apart was distinctly more difficult than registration of models from consecutive-year photos. This was due both to changes in landmarks (mainly growth of vegetation) and to the expansion of slumps beyond the area where survey ground control was obtained. In the future we may need to re-do the ground survey of some slumps or resort to the less demanding 2-D analysis described below.

2-D Modeling

To save time, I developed an abbreviated process that is adequate for 2-D registration of models and computation of changes in area and rate of main scarp migration (but not volume). For the 2-D registration process, a model was created for the year without ground control using pass points only. The result was a 3-D model with unknown scale and orientation. An approximately vertical orthophotograph of the slump was created from this model, imported into ArcMap, and georeferenced onto a true vertical orthophotograph from the year with ground control. This abbreviated process was used with 2012 photos of slump NOAT071 (which changed little between

the two photo dates), and slump NOAT069 (where ground control was not well positioned for accurate elevation computations). The abbreviated, 2-D process was also used for selected slumps in previous years (Swanson 2012a).

Aerial photographs were not taken of slumps NOAT039 and NOAT042 in 2011, but 25-cm resolution vertical aerial photographs of these slumps were taken in 2011 by Matt Nolan of University of Alaska, for another project with NPS. These photographs were used for two-dimensional (2-D) analysis of slump scarp migration as described above.

Table 3. Model accuracy parameters

Slump	Surveyed Model Pass	Surveyed Model Mean control point error[1], m x	y	z	n	2012 Model Pass	2012 Model Mean tie point error[2], m x	y	z	n
GAAR008	2011B	0.0485	0.0577	0.0254	6	2012A	0.4693	0.5019	0.5753	11
NOAT039	2010B	0.0533	0.0951	0.0417	5	2012D	0.4257	0.5337	0.2377	12
NOAT042	2010A	0.2388	0.1440	0.0321	6	2012A	2.0871	0.7642	0.6783	4
NOAT068	2010C	0.0789	0.0815	0.0724	6	2012C	0.1537	0.3557	0.1592	22
NOAT070	2010A	0.0263	0.0404	0.0410	6	2012C	0.3332	0.1573	0.3113	27
NOAT074	2011F	0.0843	0.0567	0.0627	6	2012A	0.5076	0.8905	0.0805	8
NOAT076	2011A	0.0368	0.0486	0.0340	6	2012B	0.0708	0.0602	0.0535	18
NOAT148	2010B	0.1005	0.0514	0.0908	6	2012A	0.1739	0.0641	0.0429	12
NOAT151	2011F	0.1823	0.1949	0.0989	11	2012B	0.4052	0.2050	0.2500	13
NOAT159	2011E	0.0324	0.0314	0.0308	7	2012A	0.0686	0.1089	0.1175	14
NOAT160	2011E	0.0311	0.0344	0.0384	5	2012A	0.0454	0.0718	0.0897	14
NOAT161	2010A	0.0147	0.0317	0.0231	6	2012A	0.1565	0.2139	0.1462	26
NOAT172	2010B	0.0175	0.0538	0.0228	6	2012C	0.4378	0.1745	0.0976	13
NOAT225	2010A	0.0054	0.0016	0.0146	4	2012A	0.2612	0.3252	0.1312	20
NOAT237 and 238	2011D	0.2903	0.3384	0.1934	9	2012B	0.0706	0.0292	0.0552	11
NOAT265	2011F	0.2561	0.1742	0.1577	8	2012B	0.4867	0.1947	0.2006	15

[1]Mean control point error: mean location error of all the control points. The location error of each point is the root mean square error of the computed location of the ground control point (by the bundle adjustment) relative to the location as determined by ground survey. The bundle adjustment minimizes these errors. “x” is error in the x direction (east-west); “y” is error in the y direction (north-south); “z” is error in the elevation; “n” is the number of control (ground survey) points.

[2]Mean tie point error: similar to the mean control point error, except that the locations of the points determined by the bundle adjustment of an unsurveyed model is compared to the coordinates of tie points (common landmarks) as computed by bundle adjustment on the surveyed model.

Satellite Images

To provide a longer historical perspective on slump growth, the area of each slump was measured by manually digitizing its outline on IKONOS satellite imagery (1 m resolution) taken in 2007 or 2008.

Data Analysis

The 3-D models were used to create orthophotographs and cross-sectional diagrams, and to calculate slump area, main scarp height, slope, and volume change. (An orthophotograph has a vertical perspective, and all distortions due to perspective and elevation have been removed, like a map.) To

calculate change in slump area and rate of main scarp migration, the trace of the main scarp was drawn along the uppermost large extensional fracture if an obvious vertical face was not present.

Orthophotographs of the slumps in the figures in this report are all oriented so that the main scarp of the slump is on the left side or the top of the figure and downslope is to the right or bottom of the figure. A north arrow is provided to indicate cardinal orientation.

Slumps are constantly changing through the thaw season, and photographs were taken on different dates. Thus a method was needed to correct observed amounts of change between photo dates for the length of time and warmth of the weather between the dates. The sum of thaw degree-days (sum of degree-days greater than 0° C, also known as the "thawing index") has been used for many years as a predictor of depth of seasonal thaw (e.g., US Army Corps of Engineers 1950). I reasoned that since frozen material is continuously exposed in the main scarp of an active retrogressive thaw slump, the amount of advance of the scarp during some fixed time interval should (all else being equal) be approximately proportional to the sum of thaw degree-days during that period. This provides a means to normalize the rate of thaw observed during time intervals of different lengths and in different parts of the thaw season.

Thaw degree-days were computed using the Noatak RAWS weather station, which is centrally located in the study area (Fig. 1), at approximately the same elevation as the study sites, and has records for the summer months during the years of this study. The average sum of thaw degree-days during the period 2010-12 was 1317 °C-days, somewhat higher than the long-term average of 1237 °C-days (Fig. 2). The sum of thaw degree-days was computed for the time interval between each slump sampling event and reported with the slump activity data to help understand the effect of the length of time and warmth of the season on slump behavior.

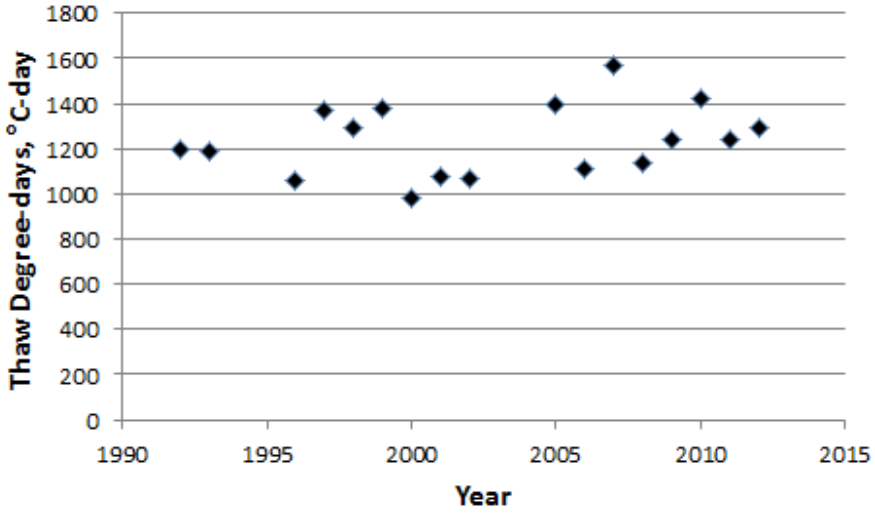

Figure 2. Annual sum of thaw degree-days (base temperature 0°C) at the Noatak RAWS weather station for the station's entire period of record (1992-2012, missing 1994-95 and 2003-04). The average of all available years was 1237 °C-days; for 2010-2012 (the time of our slump 3-D models) the average was 1317 °C-days; and for 2007-2012 (the time of our slump area measurements) the average was 1318 °C-days.

The time interval between our samples was more than one year, because our samples were mostly in June of 2010, July of 2011, and September of 2012. Meanwhile, we would like to know the amount of main scarp retreat in a typical year. Thus I adjusted the observed main scarp retreat distances as follows. The maximum scarp retreat distance (as measured on orthophotographs) of each slump between sample dates was divided by the number of thaw degree-days observed for that time period at the Noatak RAWS, to obtain a rate of retreat per thaw-degree day. Then this rate was multiplied by 1317 °C-days, the average annual degree-day sum for the period 2010-2012, to obtain an adjusted distance for a single typical season.

Results and Discussion

Between 2011 and 2012 most of the study slumps continued to grow at significant rates, though in nearly all cases the rate of growth was slower in 2011-2012 than in 2010-2011 (Table 4). The rate of main scarp retreat in 2011-2012, normalized to the equivalent of one typical thaw season, ranged from just 2 or 3 meters in the less active slumps up to 33 m in the most active slump. In all cases except one (NOAT148) the retreat rates were less in 2011-2012 than in 2010-2011. The fastest rates of retreat were generally in slumps with vertical scarps that migrated by the "fall and flow" mechanism (Fig. 3). The volume lost in the vicinity of the main scarp for several of the slumps totaled more than 10,000 m^3 during the 2011-2012 period; NOAT265 was the most active slump with over 40,000 m^3 lost. As in the previous year (Swanson, 2012a), many of the slumps had a zone of sediment accumulation just below the main zone of subsidence, where the volume gain was typically less than half of what was lost above (Table 4).

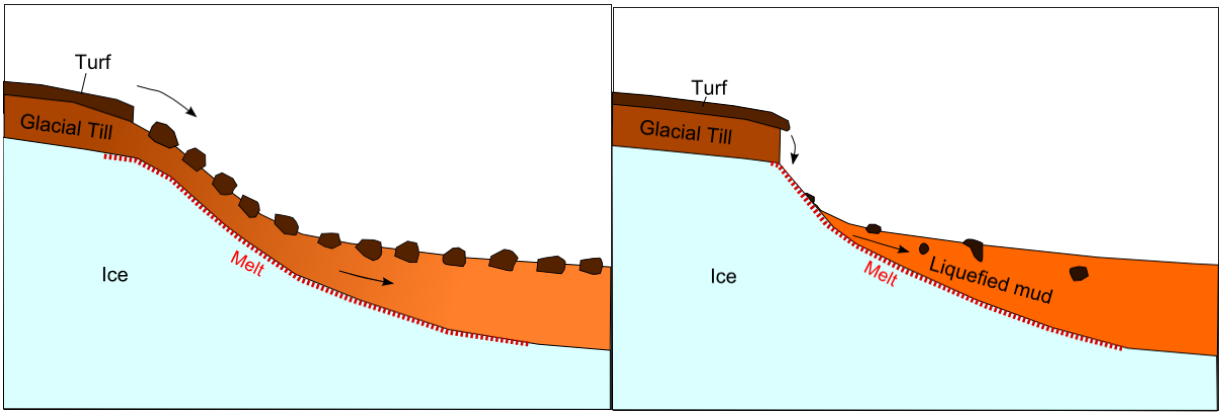

Figure 3. Slump modes of scarp retreat . Extensional flow (left) and fall and flow (right). For a more detailed explanation, see Swanson (2012a)

For all slumps that had subsidence volumes from the two different time intervals, the amount lost during 2011-2012 was less than what was lost in 2010-2011. Unlike the scarp retreat rates, these volumes were not normalized by thaw degree-days, but note that in all slumps with two subsidence volumes the number of thaw degree-days available was less during the 2011-12 interval than the 2010-11 interval between samples, which indicates that the decreased subsidence in 2011-2012 was *not* due to a shorter time interval between samples or cooler weather in 2011-2012. Note also that the average annual sum of thaw degree-days in 2012 (1292 °C-days) was near the average of 1318 °C-days for the period of slump area measurements (2007-2012, Fig. 2), Thus the slowing of slump growth in 2012 was probably not due to colder weather but instead to factors internal to the slumps, such as escarpments migrating to areas with lower slopes or less ice-rich material.

Table 4. Summary of slump activity, 2010-2012

Slump ID	Area in 2012, m^2	Normalized Maximum Main Scarp Retreat, m, and mode of scarp retreat[1]		Subsidence Volume Loss (Gain[2]), m^3		Maximum Subsidence, m		Sum of Thaw Degree-Days Between Sample Dates. °C-days		
		2010-2011	2011-2012	2010-2011	2011-2012	2010-2011	2011-2012	2010-2011	2011-2012	2010-2012
GAAR008	13695	24, f	10, e	3,443 (310)	617 (446)	3.2	2.2	1672	1797	3469
NOAT039[3]	50855	12, f	8, f	29,712 (2,626)		9.5		2219	1267	3486
NOAT042[3]	19566	9, f	8, f	30,675		10.4		2219	1267	3486
NOAT068	38239	31, f	29, f	15,008 (8,123)	11,628 (5,271)	4.1	4.3	1712	1806	3518
NOAT069[4]	19787	50, f	33, f	ND	ND	ND	ND	1712	1806	3518
NOAT070	55668	35, f	29, f	36,135 (9,319)	16,095	5.2	4	1712	1806	3518
NOAT071[4]	12440	2, e		ND	ND	ND	ND	ND	ND	3518
NOAT074	15275	28, f	15, e	9,710 (2,419)	3,753 (362)	3.6	2.9	1662	1806	3469
NOAT076	13457	16, f	12, e	3,484 (2,078	1,739 (579)	3.8	2.8	1662	1806	3469
NOAT148	22338	12, f	13, f	12,916 (1,221)	11,379 (2,844)	6.2	5.1	1683	1819	3501
NOAT151[4]	54481	27, f	18, f	ND	16,197 (3,186)	ND	4.9	1704	1797	3501
NOAT159	7911	14, e	4, e	3,376 (454)	439	3.9	1.9	1662	1806	3469
NOAT160	12254	8, e	3, e	2,138 (78)	454	2	1.4	1662	1806	3469
NOAT161[3]	16663	20, m	2, e	4,961 (904)		2.4		1662	1806	3469
NOAT172	21891	9, f	7, f	8,079 (1,494)	4,320 (193)	7.2	4.4	1728	1806	3534
NOAT225[3]	12648	4, m		747 (293)		2.1		ND	ND	3518
NOAT237	16636	28, f	22, f	10,627 (2,489)	9,040 (1,177)	3.8	3.4	1666	1819	3484
NOAT238	5462	16, f	3, e	1,444 (527)	1,208	3.7	2.2	1666	1819	3484
NOAT265[4]	36651	ND	21, f	ND	48,960 (11,414)	ND	16.8	ND	1852	ND

[1]Predominant mode of main scarp migration (see Fig. 3): e – extensional flow, f – fall and flow, m – mixed (both extensional and fall and flow).

[2]"Loss" is the volume of subsidence in the upper subsidence zone just below the main scarp; "Gain" is the increase in volume of material in the zone of sediment accumulation just below the loss area that was observed in many slumps.

[3]NOAT039, NOAT042, and NOAT161 had only 2-D analysis of 2011 data, so the Subsidence Volume and Maximum Subsidence values refer to the interval 2010-2012. NOAT225 had no photo in 2011 so the subsidence values also refer to the 2010-2012 interval.

[4]ND – No data. In the case of NOAT069, NOAT071, and NOAT151, subsidence data are missing because only 2-dimensional analysis has ever been made of these slumps. For NOAT265 monitoring was begun in 2011 so no 2010-2011 change data are available.

Plots of slump area vs. time made with our 3-D model data, combined with areas measured on 2007-2008 IKONOS satellite images, give a picture of slump growth over a longer term (Figs. 4-7). Slumps are grouped by size in these figures; note the change in scale between the figures. All of the slumps except NOAT148 show a slight decline in the rate of area growth in 2011-12 as compared to 2010-11, similar to what was noted above with respect to slump scarp migration rates. Two of the slumps (NOAT247 and NOAT248, Fig. 7) have grown little since 2008, while two others (NOAT071 and NOAT225, Fig. 6) grew between 2008 and 2010 and then stabilized thereafter at an area of about 1 ha (10,000 m^3). The other slumps had growth rates between 2007 or 2008 and 2010 that were similar to those measured in 2010-12. If we extrapolate the observed slump area growth rates from our first observations interval (2008 to 2010 for most of the slumps) linearly back in time, the intercepts suggest that the time of inception for all of the slumps, regardless of size, was between 1996 and 2006 (Fig. 8).

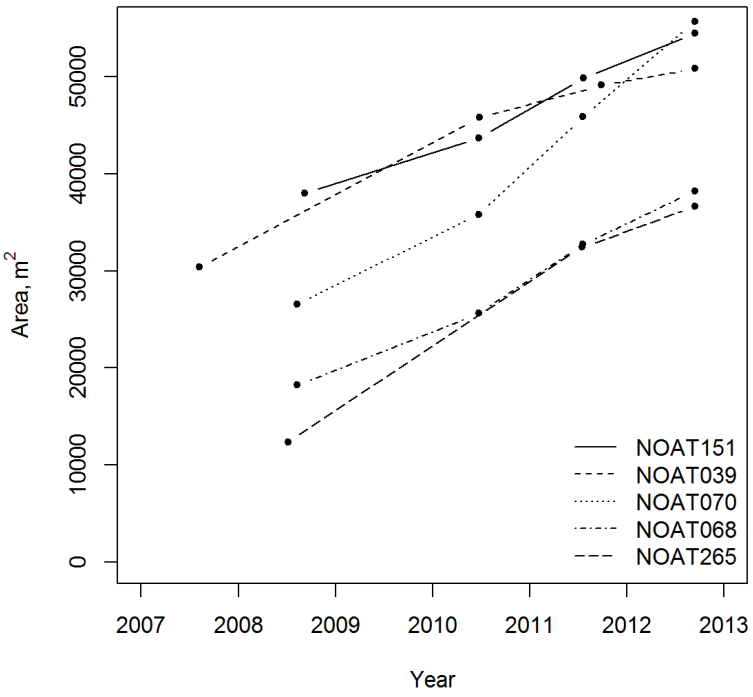

Figure 4. . Slump area growth 2007-2012 for the largest (3-5 ha) slumps.Here and in subsequent figures 5, 6, and 7, the year tic marks on the x-axis mark the position of January 1 for the year indicated.

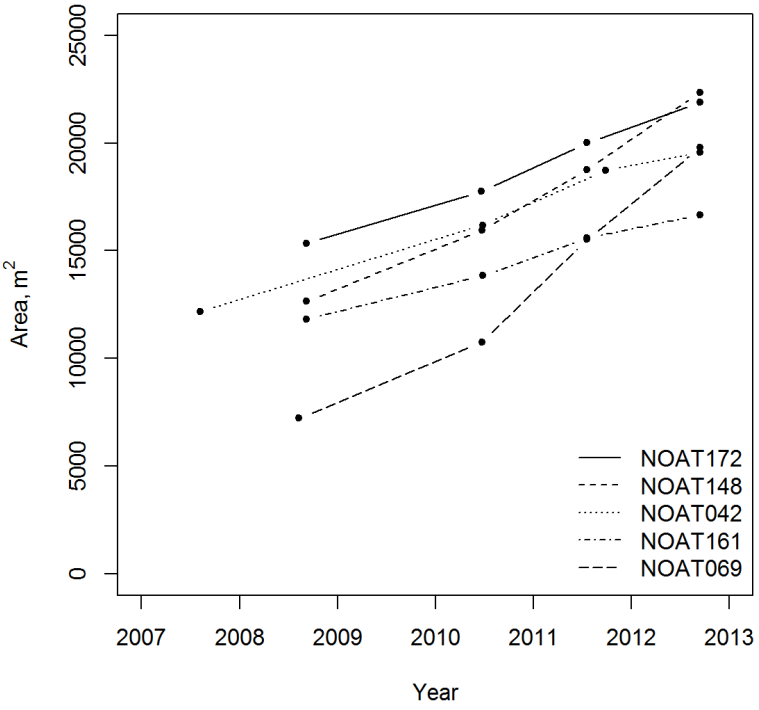

Figure 5. . Slump area growth 2007-2012 for large (1-2 ha) slumps.

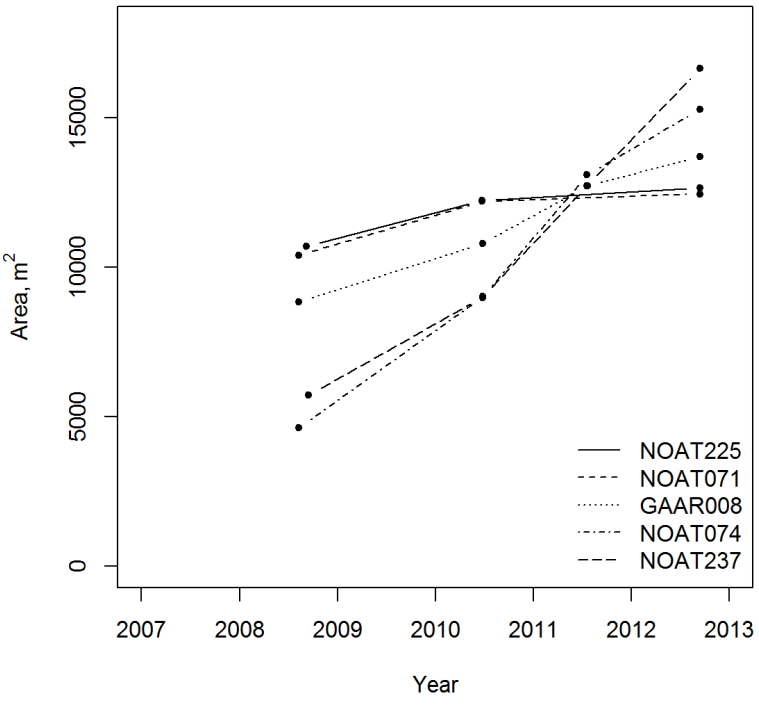

Figure 6. . Slump area growth 2008-2012 for mid-sized (about 1 ha) slumps.

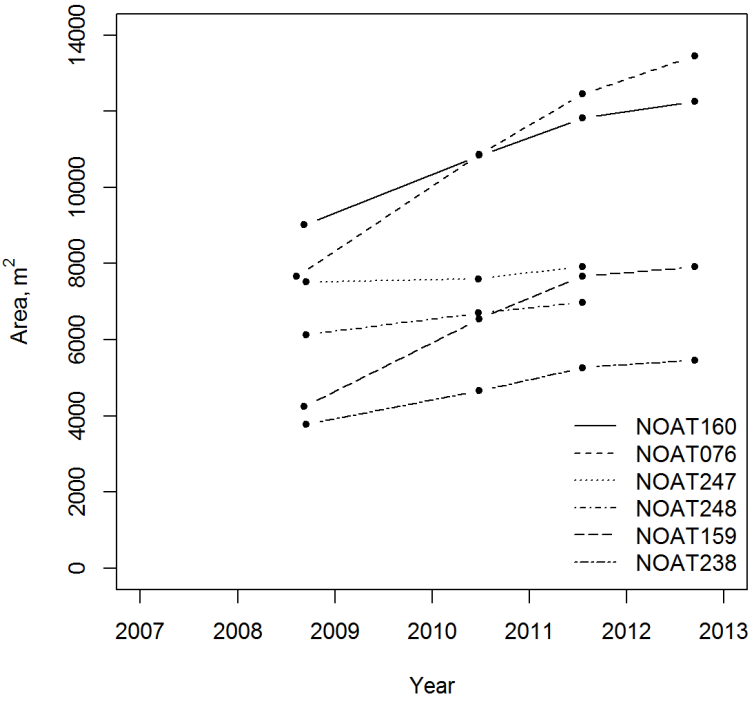

Figure 7. Slump area growth 2008-2012 for the smallest (0.5 to 1 ha) monitored slumps.

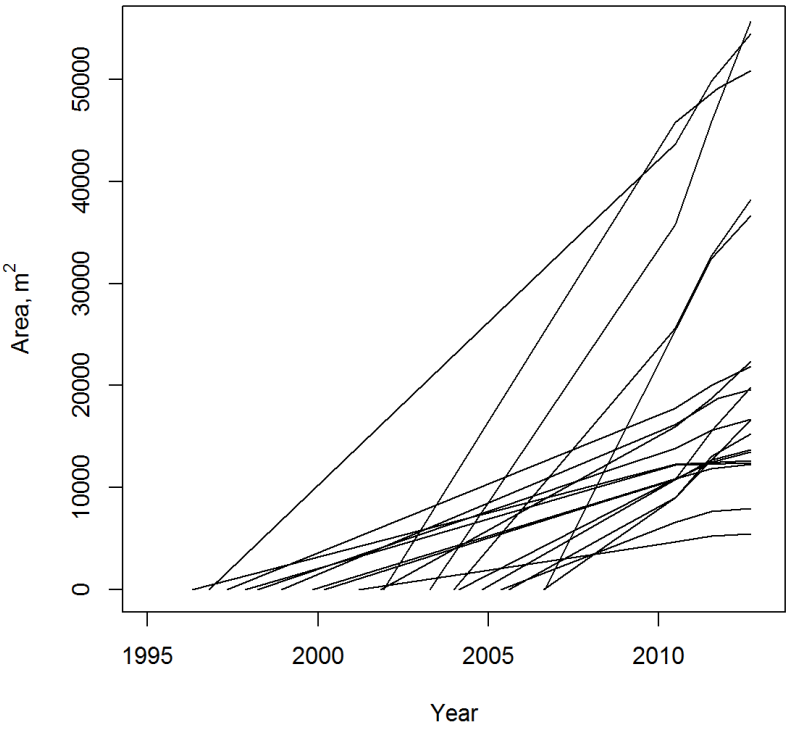

Figure 8. . Extrapolation of slump growth rates back to inception dates. Data are the same as in Figs. 4-7, with the rate of slump growth during the first observed time interval (in most cases 2008 to 2010) extrapolated back to the x-intercept. Slumps NOAT247 and NOAT248 were omitted because they had largely stabilized prior to 2008.

Though we lack data for an entire slump growth cycle, I would expect a sigmoidal slump growth pattern: 1) initial slow growth as the main scarp develops and becomes wider, 2) an extended period of rapid growth, and 3) a final slowing of growth as the main scarp becomes less vertical before stabilization. Our monitored slumps were chosen mainly by searching the 2007-2008 IKONOS satellite images for large, active slumps. Thus, these slumps were presumably in the rapid growth phase (2) at that time. Thus it is not surprising that in 2010-2012 these slumps were either continuing their rapid growth phase (2) or slowing as they stabilized (phase 3).

During fieldwork since 2010 in these clearly slump-prone areas, I have encountered very few large or active new slumps, i.e. slumps not present in 2007-2008 but now entering a period of rapid growth. Nor have I received staff reports of any such large or active new slumps. Analysis of aerial photographs from the year 1977 in the vicinity of the monitored slumps (Swanson and Hill 2011, Swanson 2012b) revealed active slumps present at that time, but all grew little or not at all up to the present (i.e. they stabilized around 1977). These are also the only stabilized slump scars currently visible, suggesting a period of quiescence between 1977 and the current period of active growth beginning in the late 1990s. The 1990s was a time of warming permafrost temperatures and permafrost degradation at many places in northern Alaska due to warm temperatures and thick snow cover (Jorgenson et al. 2006, Osterkamp 2005). Permafrost temperatures appear to have stabilized somewhat in the 2000 decade, probably due to slightly lower temperatures associated with changes in the Pacific Decadal Oscillation (Wendler et al. 2012). However, the exceptionally warm summer of 2004 appears to have initiated some permafrost thaw in spite of overall cooler temperatures during the 2000 decade (Swanson 2012b). Thus an active cycle of RTS growth began in the late 1990s and early 2000s that is currently continuing but apparently slowing as it runs its natural course.

Our plan is to continue monitoring the slumps on our current list, gradually dropping those that become inactive, while continuing to search for new slumps on imagery and from staff report from the field. This would allow us to test whether the current phase of slump activity is in fact running its course and also keep us prepared to detect a new phase of slump activity if one were triggered by future warming.

Illustrations of the slumps and a brief description of growth trends are given in Fig. 9 through 26 below.

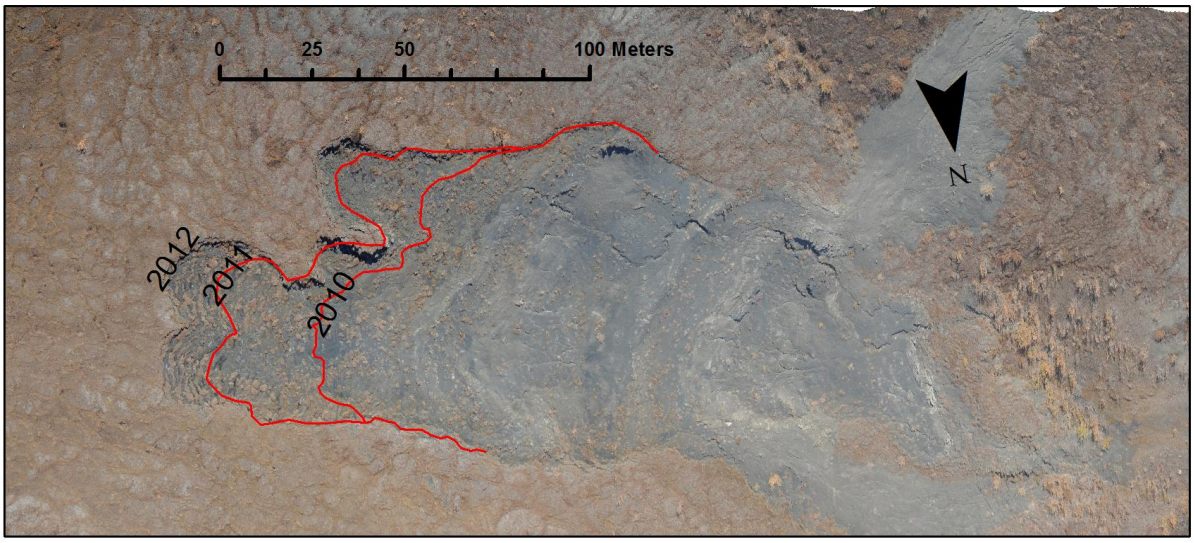

Figure 9. Orthophotograph of slump GAAR008 on 10 Sept 2012. This slump showed signs of slowing growth in 2011-12: less scarp retreat than in the preceding year and a change in scarp morphology from vertical (the fall-and-flow growth mechanism) to rounded (extensional flow growth).

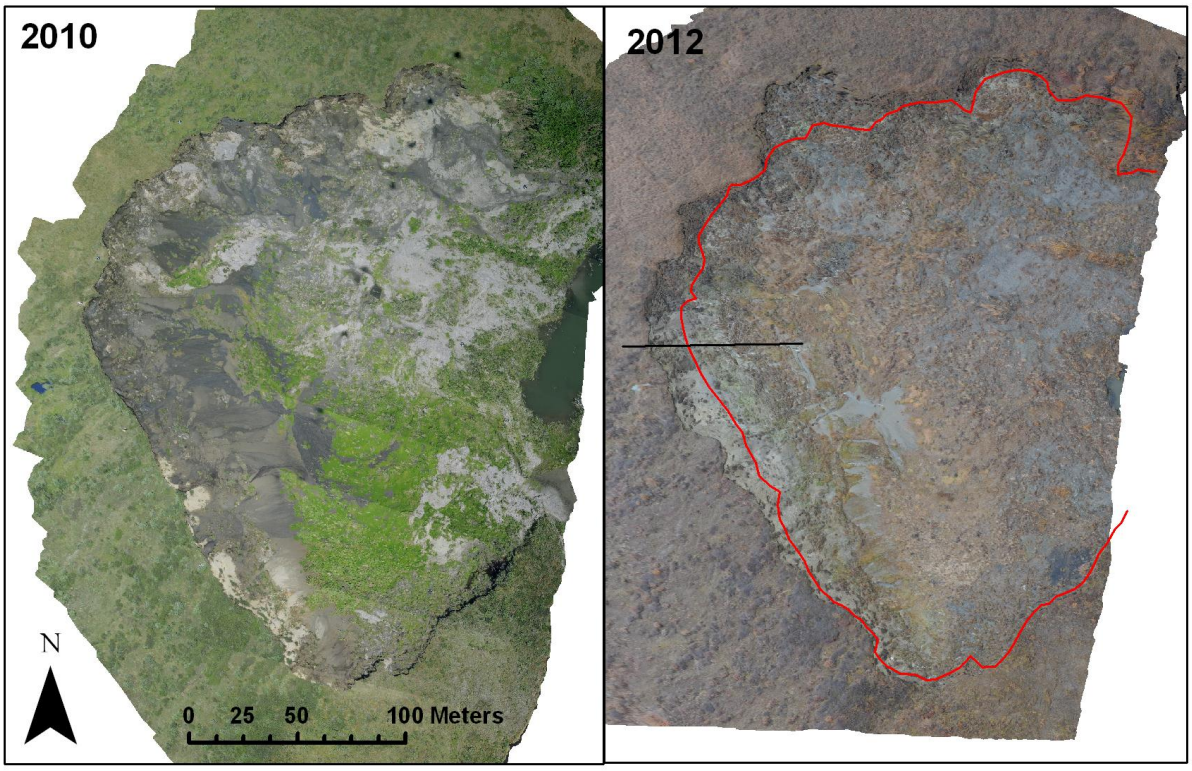

Figure 10a. Orthophotographs of slump NOAT039 on 24 June 2010 (left) and 11 Sept 2012 (right). The location of the cross-section in Fig. 10b is shown as a black line and the trace of the 2010 main scarp as a red line on the 2012 photo. While the total scarp retreat was less than 20 m over most of its length over the two years, the volume loss was quite large (nearly 30,000 m^3) due to the large size of this slump and its tall escarpment (up to 10 m).

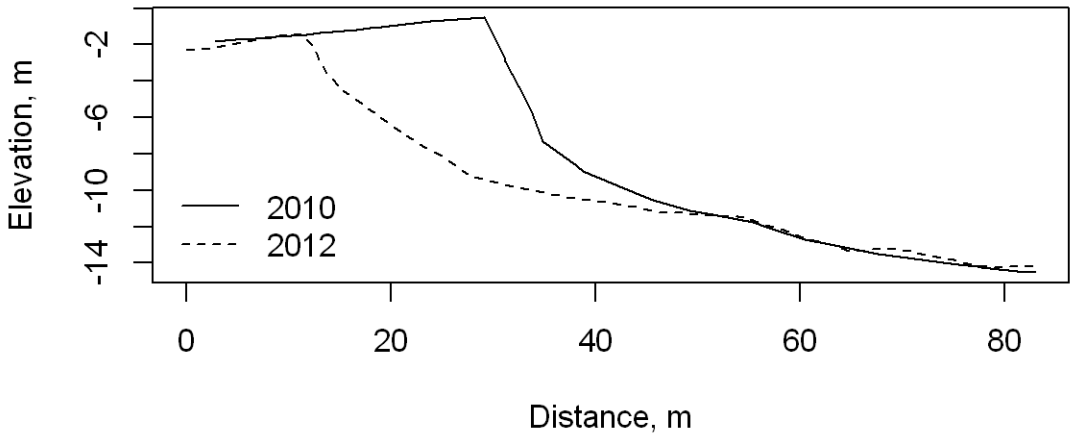

Figure 10b. Cross-sections of slump NOAT039 on 24 June 2010 and 11 Sept 2012. The location of the cross-section is show in black on Fig. 10a.

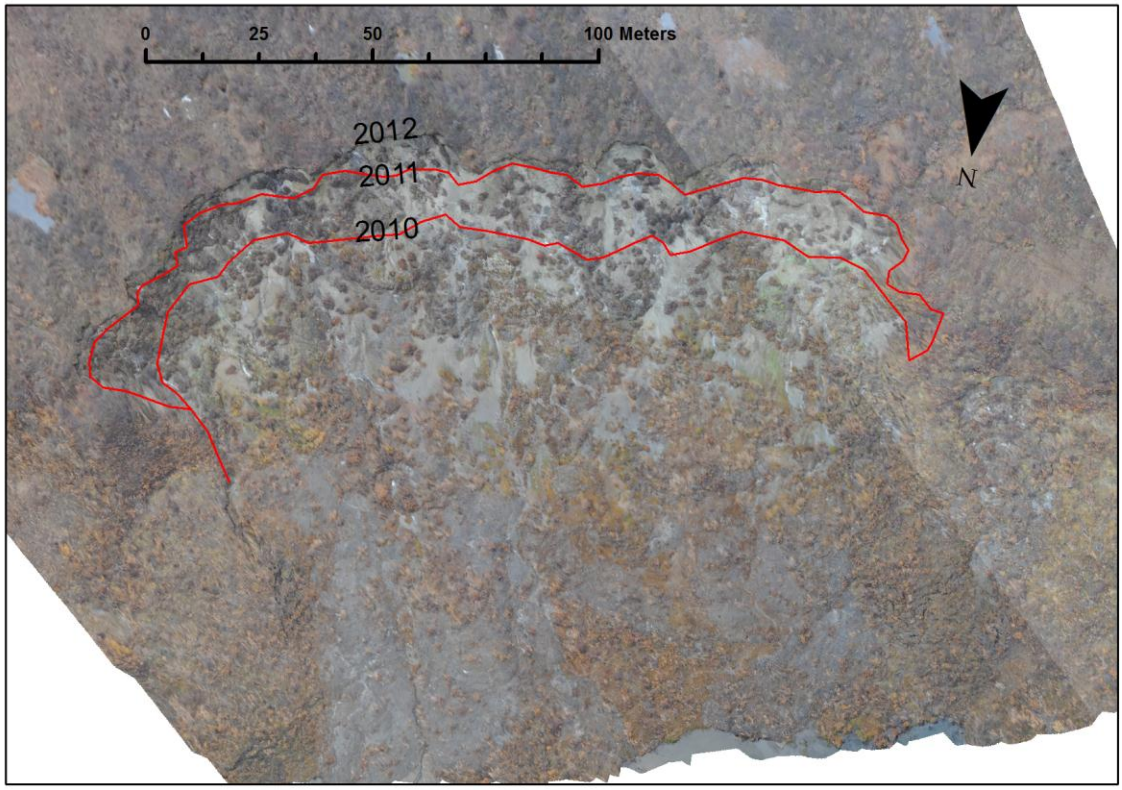

Figure 11. Orthophotograph of slump NOAT042 on 11 Sept 2012. This slump, located near NOAT039 and in similar deposits, also had a tall scarp that retreated a modest amount but resulted in significant (about 30,000 m^3) subsidence over the two seasons.

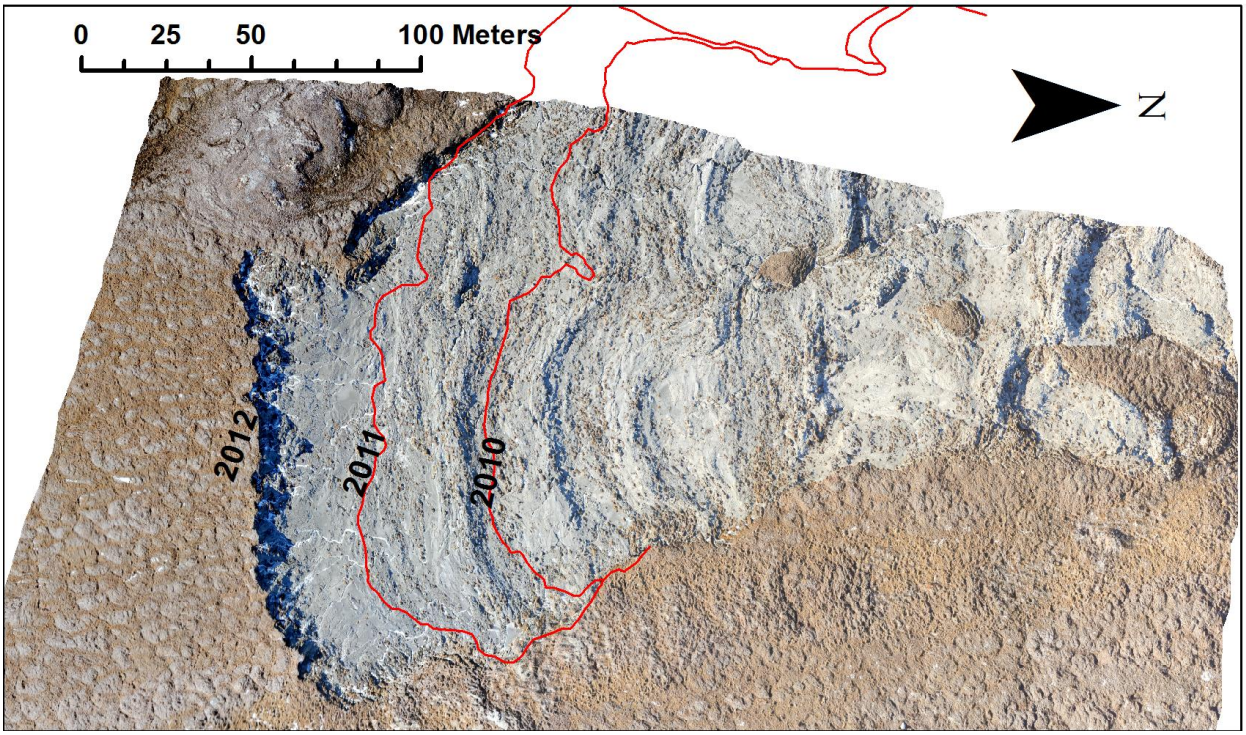

Figure 12. Orthophotograph of slump NOAT068 on 10 Sept 2012. This slump continued to grow rapidly, with 30 to 40 m of scarp retreat between 2011 and 2012.

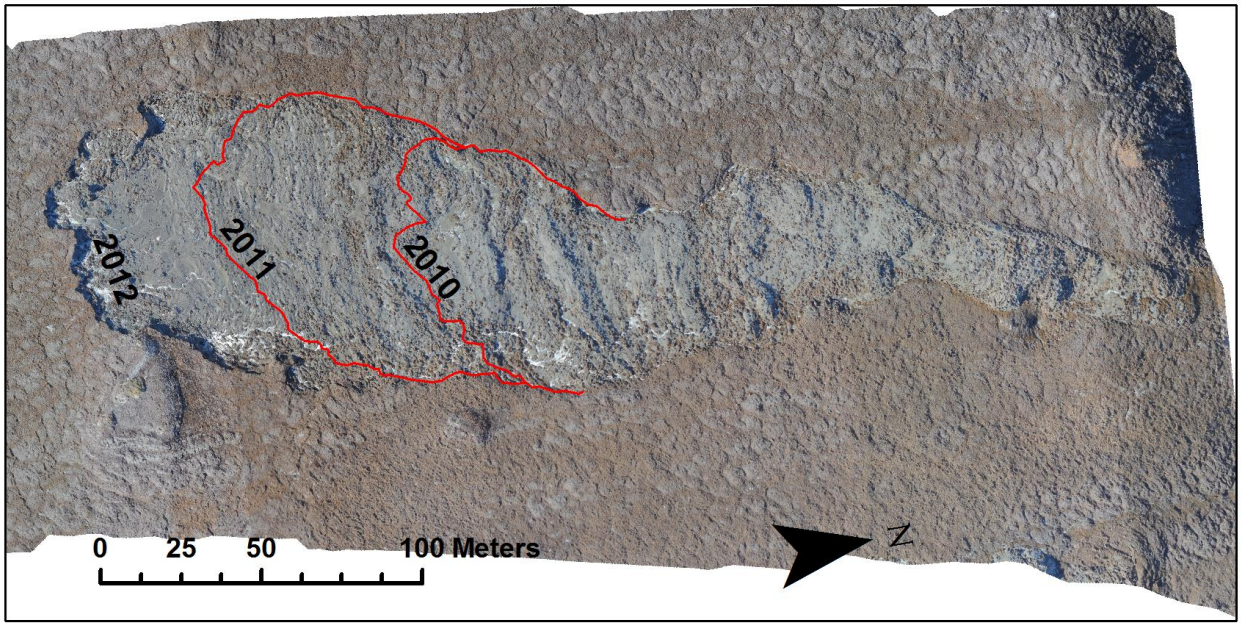

Figure 13. Orthophotograph of slump NOAT069 on 10 Sept 2012. This slump had our fastest rate of scarp retreat, amounting to over 100 m between June 2010 and Sept 2012.

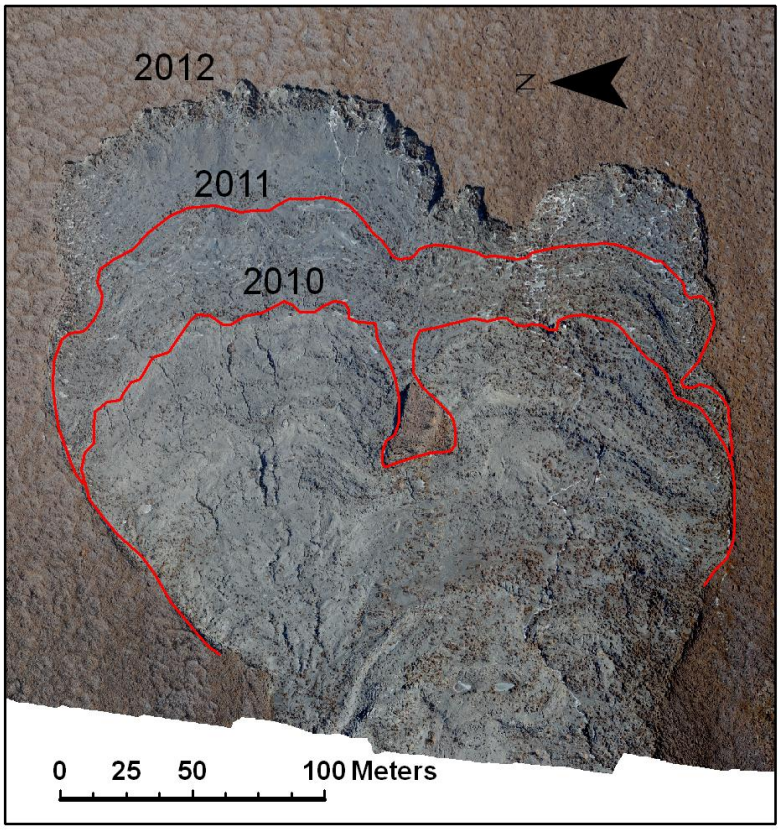

Figure 14. Orthophotograph of slump NOAT070 on 10 Sept 2012. This slump was very active, with a vertical main scarp migrating 30 to 40 m since 2011 by the “fall and flow” mechanism.

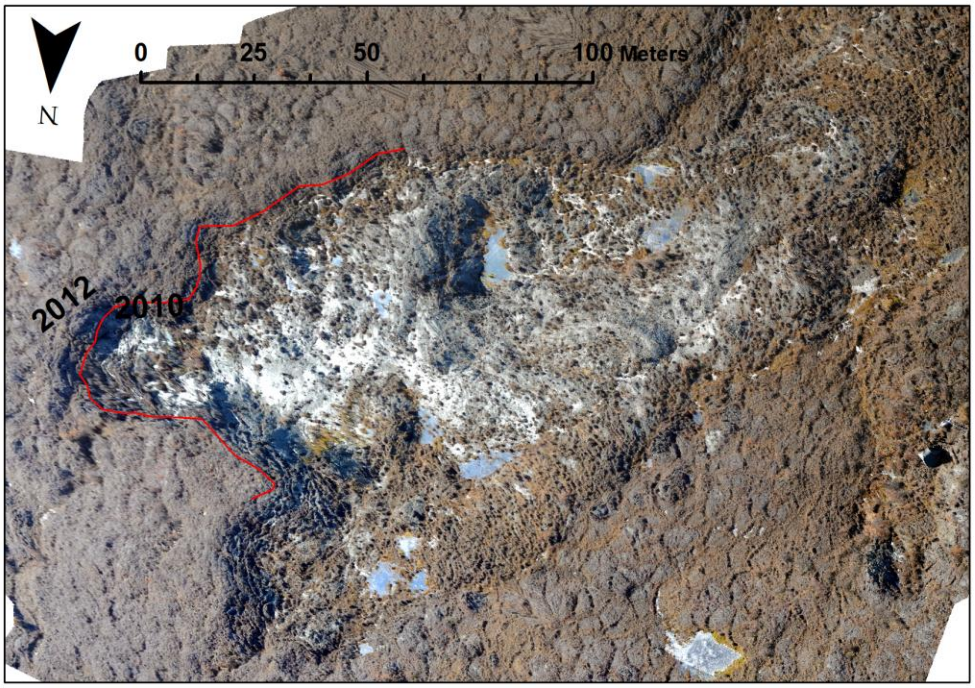

Figure 15. Orthophotograph of slump NOAT071 on 10 Sept 2012. This slump displayed little change since 2010.

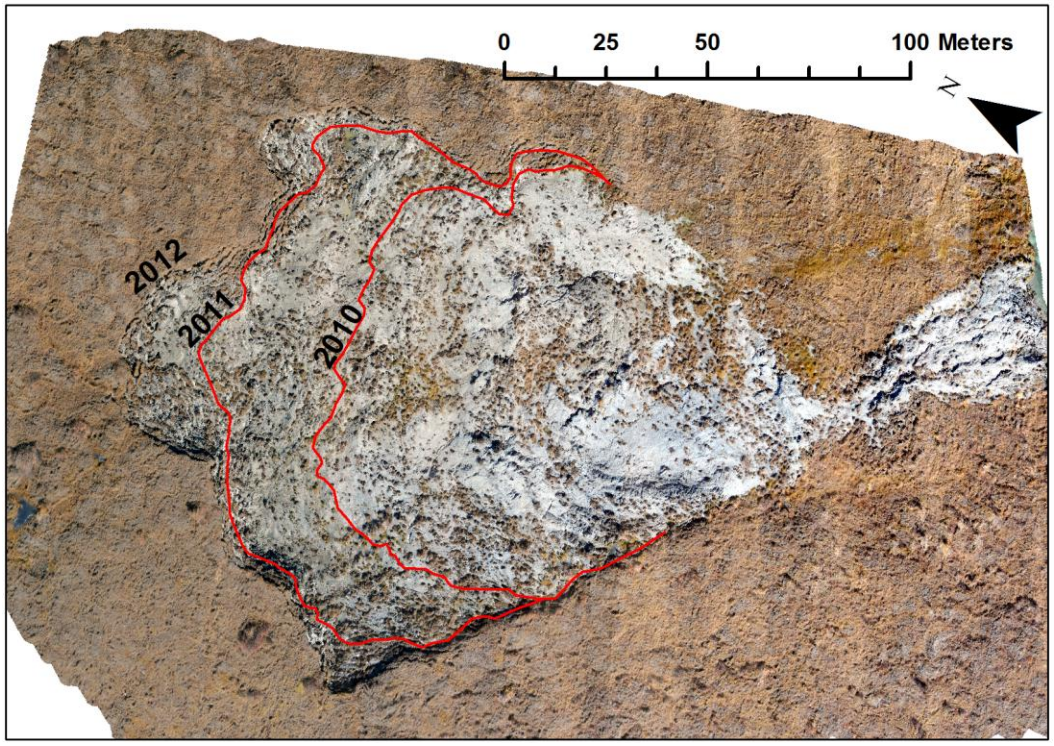

Figure 16. Orthophotograph of slump NOAT074 on 10 Sept 2012. This slump showed signs of slowing growth, with less scarp retreat in 2011-12 than 2010-11 and a main scarp morphology that changed from vertical in 2011 (fall-and-flow growth mechanism) to rounded (extensional flow mechanism) in 2012.

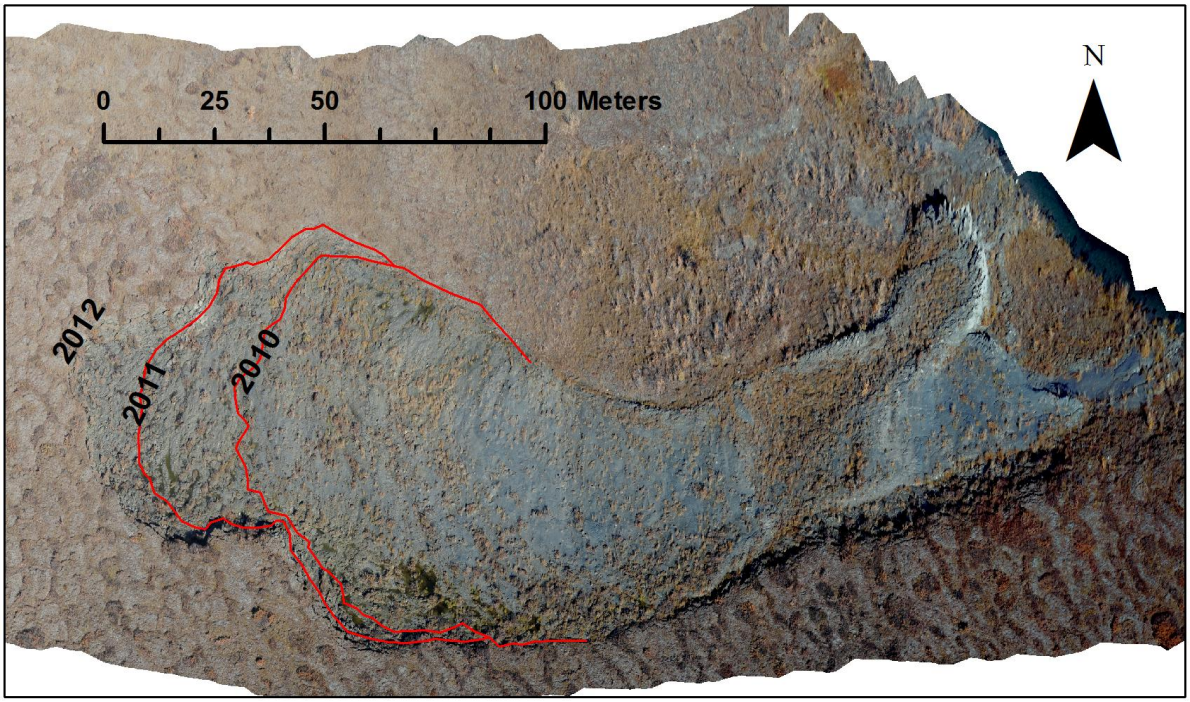

Figure 17. Orthophotograph of slump NOAT076 on 10 Sept 2012. The vertical main scarp in 2011 became rounded in 2012 and changed to the extensional flow migration mechanism.

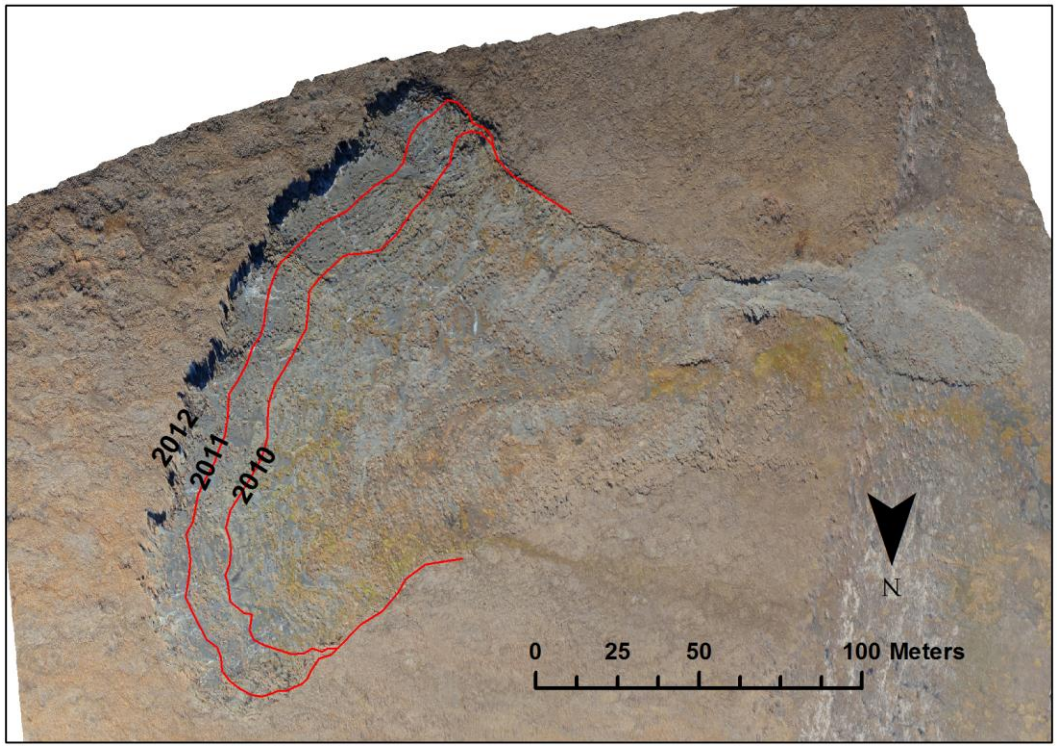

Figure 18. Orthophotograph of slump NOAT148 on 10 Sept 2012. This slump continued steady growth, with a tall (about 5 m), vertical main scarp.

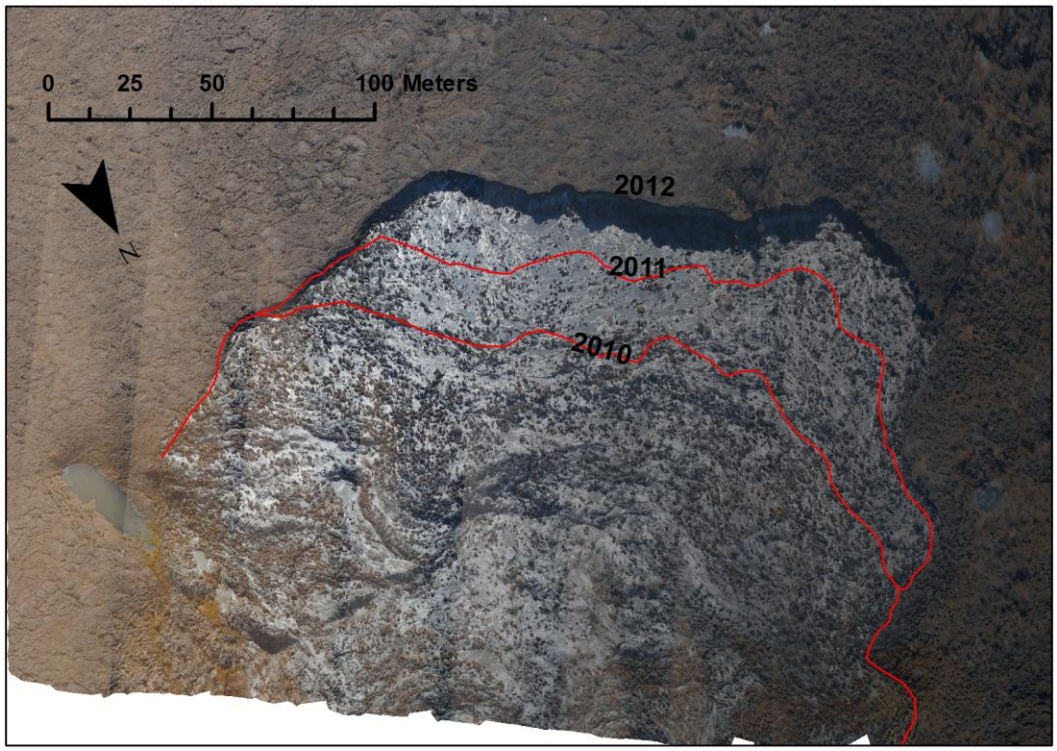

Figure 19. Orthophotograph of slump NOAT151 on 10 Sept 2012. This large slump (5.5 ha) grew rapidly, with over 16,000 m^3 of subsidence along a 5 m-tall, vertical main scarp that exposed ground ice.

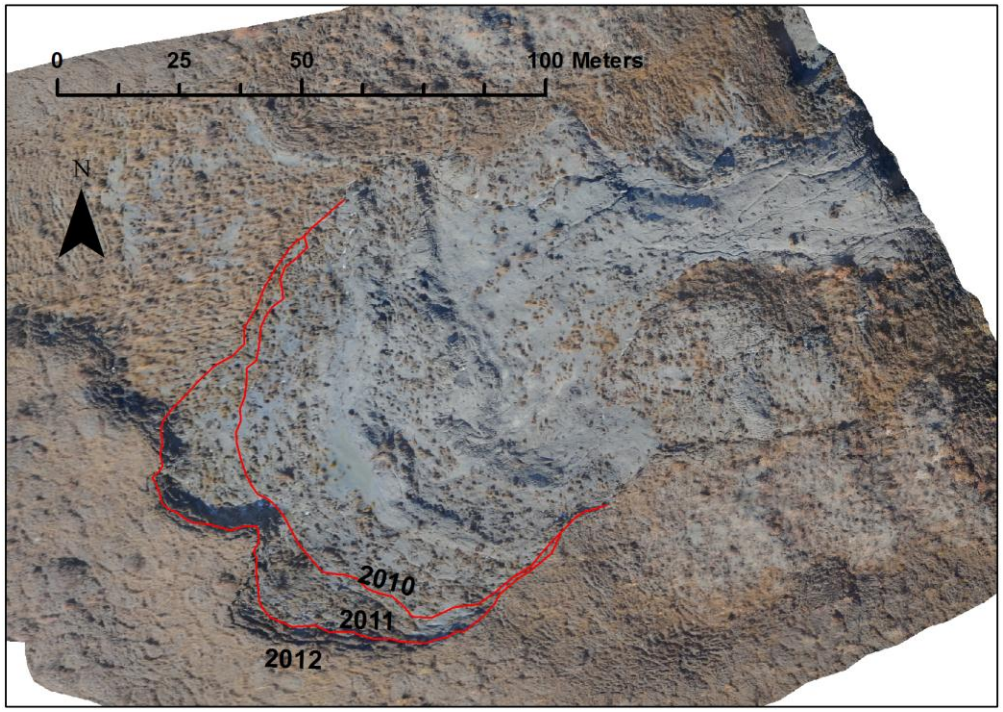

Figure 20. Orthophotograph of slump NOAT159 on 10 Sept 2012. The main scarp of this slump had become rounded during the previous time interval (2010-11) and remained that way during 2011-12. Very little new growth occurred in 2011-12.

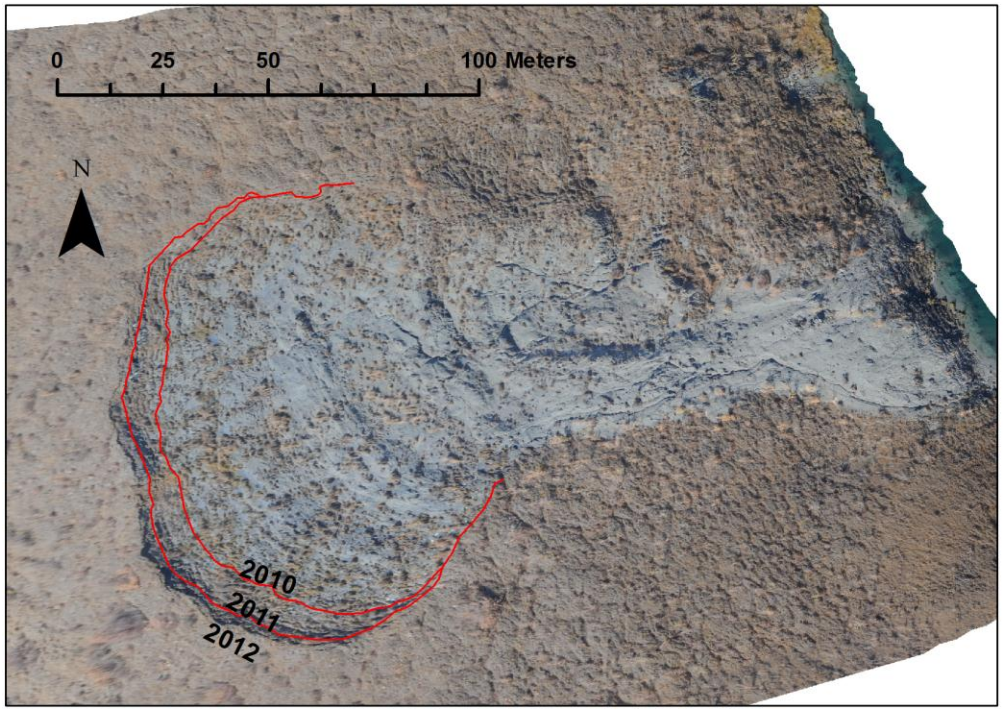

Figure 21. Orthophotograph of slump NOAT160 on 10 Sept 2012. The scarp on this slump changed from vertical to rounded during 2010-11 and remained that way through 2012, adding only a little additional area by the extensional flow growth mechanism.

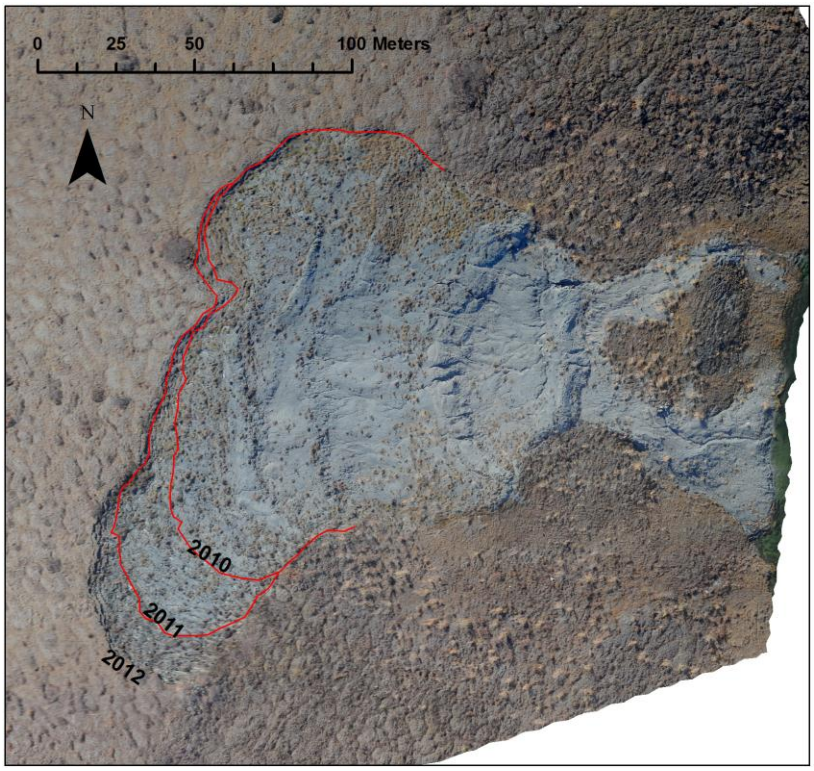

Figure 22 . Orthophotograph of slump NOAT161 on 10 Sept 2012. Most of the main scarp was stable on this slump except the southwest corner, where it migrated up to 16 m by extensional flow.

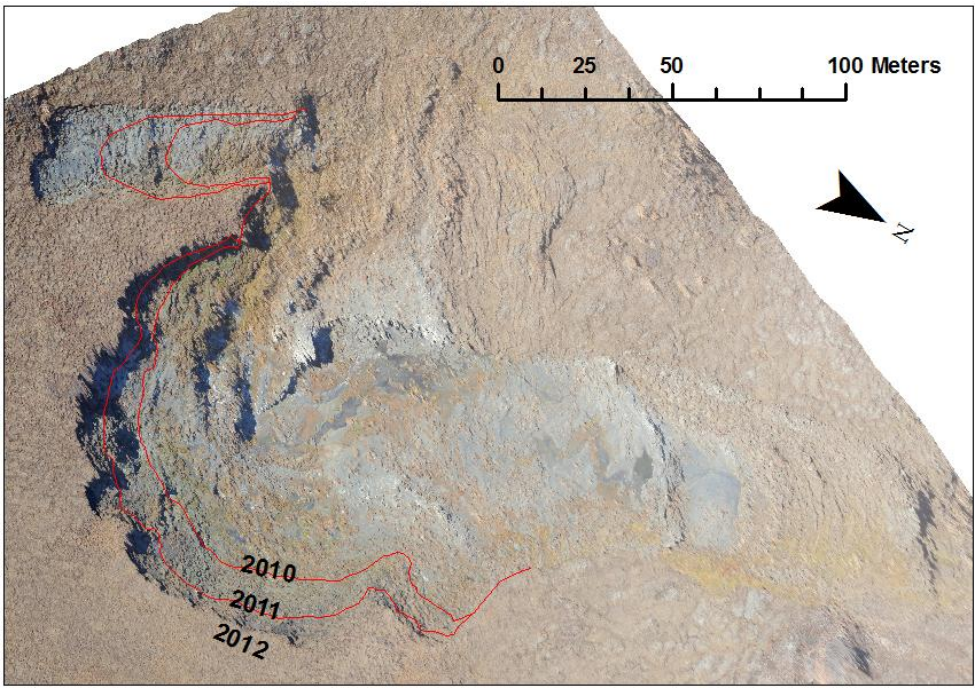

Figure 23 . Orthophotograph of slump NOAT172 on 10 Sept 2012. The main scarp of this slump was quite high (8 m), but it had become more gradual than in previous years and the spectacular ice exposures of the past were obscured. The rate of growth 2011-12 was slower than in the preceding period, except in the shallow side slump in the upper part of this photo.

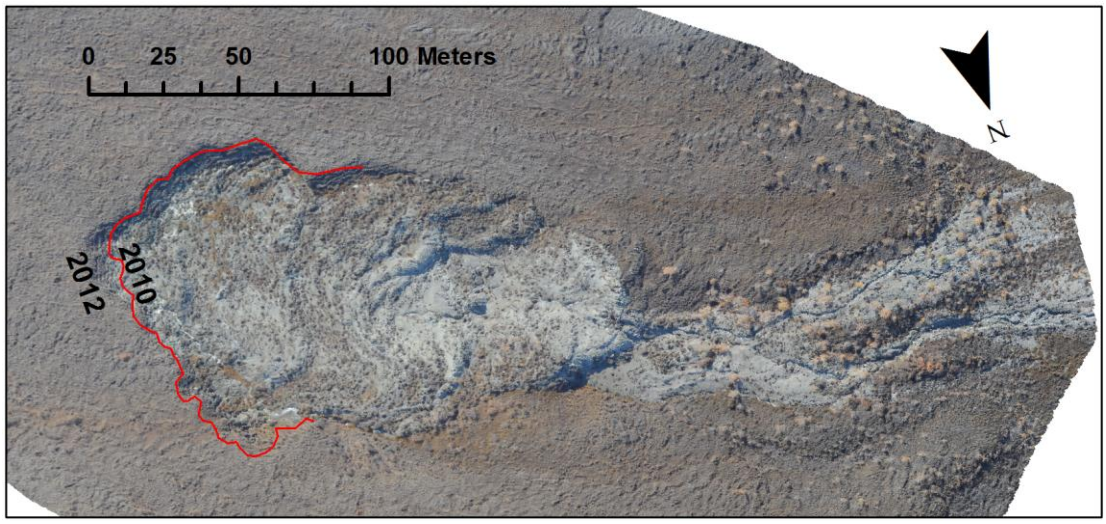

Figure 24. Orthophotograph of slump NOAT225 on 10 Sept 2012. This slump had a rounded main scarp and grew very little between 2010 and 2012.

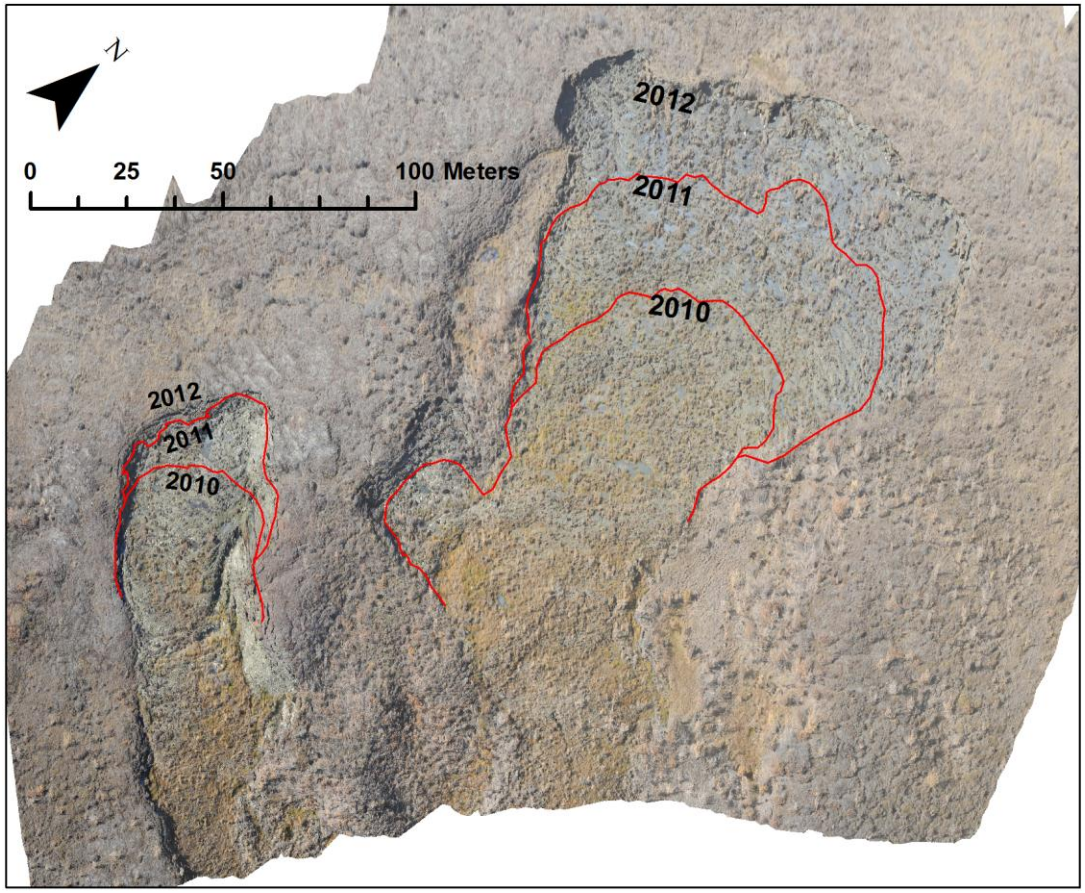

Figure 25. Orthophotograph of slump NOAT237 (right) and NOAT238 (left) on 10 Sept 2012. NOAT237 continued its rapid growth with a near-vertical main scarp that nonetheless appeared to expose little ice – foreshadowing a slowdown of growth in the future. Growth has progressed beyond the limits of a previous generation of slumping (visible as a low area just to the left of the active slump) into undisturbed material. NOAT238 (left) continued to subside in the area that had slumped in previous years, but the main scarp advanced little and by the extensional flow mechanism.

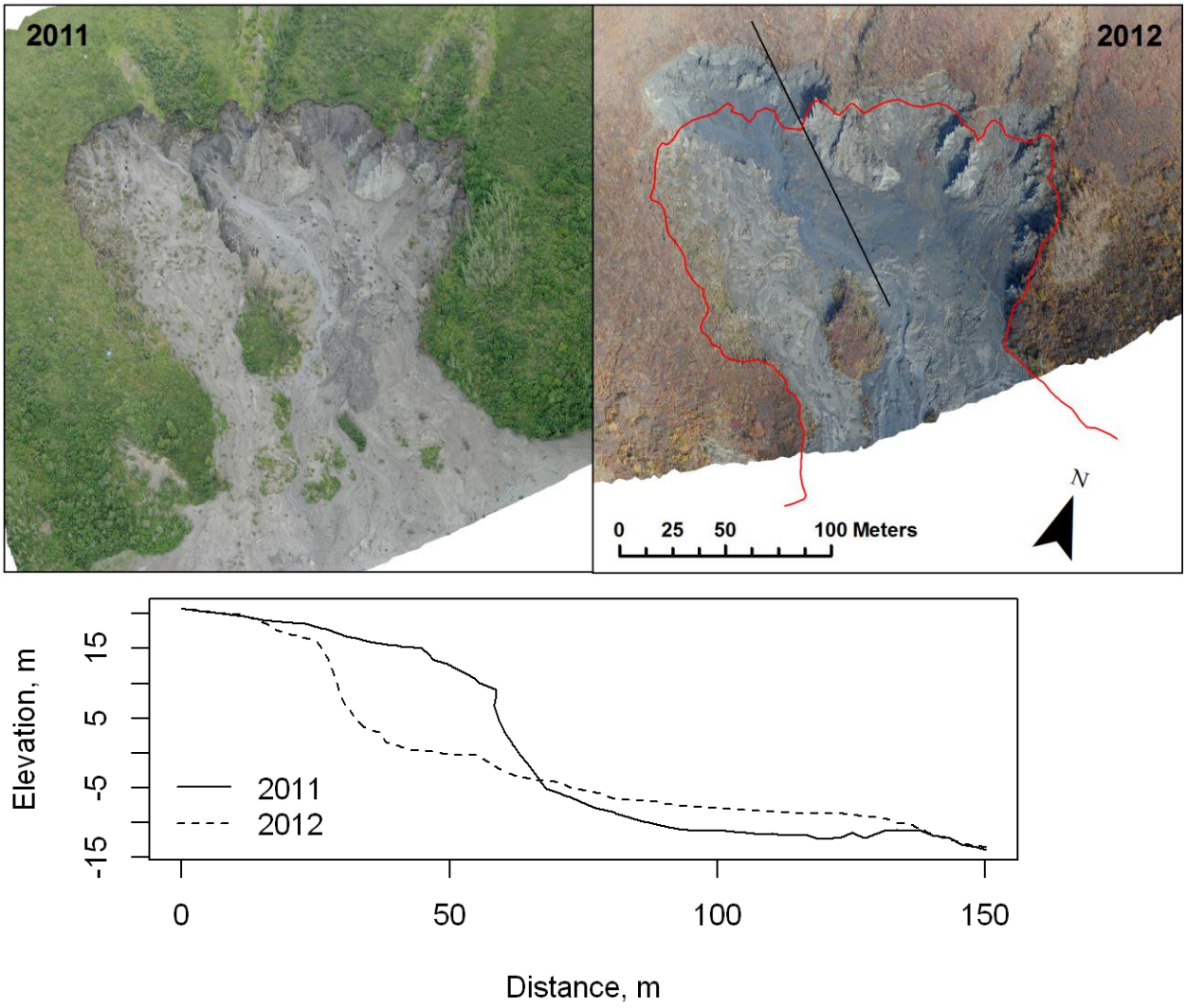

Figure 26. Orthophotographs and cross-section of slump NOAT265 on 15 July 2011 (left) and 11 Sept 2012 (right). The location of the cross-section is shown as a black line and the trace of the 2011 escarpment as a red line on the 2012 photo. This large and very active slump had a main scarp about 15 m high that migrated 15 to 30 m between 2011 and 2012, resulting in subsidence of about 50,000 m^3 in the upper part, balanced in part by a gain of about 10,000 m^3 below. The missing volume, which consisted of both sediment and water from melting of ground ice, was shed into the adjacent Noatak River.

Literature Cited

Balser, A. W., W. B. Bowden, J. B. Jones, M. N. Gooseff, D. M. Sanzone, A. Bouchier, and A. Allen. 2007. Thermokarst distribution in the Noatak Basin, Alaska: increased frequency and correlations with local and regional landscape variables. American Geophysical Union, Fall Meeting 2007, abstract #C32A-08.

Beltran, L., D. M. Cruden, E. Krauter, G. Lefèvre, G. I. Ter-Stepanian, and Z. Zhouyuan. 1993. Multilingual landslide glossary. The International Geotechnical Societies' UNESCO Working Party for World Landslide Inventory. Bi-Tech Publishers, Richmond, B.C. Canada. 50 pp. Available from: http://www.cgs.ca/pdf/heritage/Landslide%20Glossary.pdf (accessed 29 Dec 2011).

Bowden, W. B., M. N. Gooseff, A. Balser, A. Green, B. J. Peterson, and J. Bradford. 2008. Sediment and nutrient delivery from thermokarst features in the foothills of the North Slope, Alaska: Potential impacts on headwater stream ecosystems. Journal of Geophysical Research, Vol. 113, G02026, 12 pp

Burn, C. R., and A. G. Lewkowicz. 1990. Retrogressive thaw slumps. Canadian landform examples – 17. The Canadian Geographer 34(3):273–276.

Crosby, B. T. 2009. The interplay between storage and delivery: an examination of temporally varying sediment flux to the Selawik River from an enormous retrogressive thaw slump, northwest Alaska. Geological Society of America Abstracts with Programs, Vol. 41, No. 7, p. 574.

Jorgenson, M. T., Y. L. Shur, and E. R. Pullman. 2006. Abrupt increase in permafrost degradation in Alaska. Geophysical Research Letters 33:L02503.

Jorgenson, T., K. Yoshikawa, M. Kanevskiy, Y. Shur, V. Romanovsky, S. Marchenko, G. Grosse, J. Brown, and B. Jones. 2008. Permafrost characteristics of Alaska. Proceedings of the Ninth International Conference on Permafrost. University of Alaska Fairbanks, Institute of Northern Engineering.

Kokelj, S. V., R. E. Jenkins, D. Milburn, C. R. Burn, and N. Snow. 2005. The influence of thermokarst disturbance on the water quality of small upland lakes, Mackenzie Delta region, Northwest Territories, Canada. Permafrost and Periglacial Processes 16:343-353.

Lacelle, D., J. Bjornson, and B. Lauriol. 2010. Climatic and geomorphic factors affecting contemporary (1950-2004) activity of retrogressive thaw slumps on the Aklavik Plateau, Richardson Mountains, NWT, Canada. Permafrost and Periglacial Processes 21:1-15.

Lantuit, H., and W. H. Pollard. 2008. Fifty years of coastal erosion and retrogressive thaw slump activity on Herschel Island, southern Beaufort Sea, Yukon Territory, Canada. Geomorphology 95:84-102.

Lantz, T. C., and S. V. Kokelj. 2008. Increasing rates of retrogressive thaw slump activity in the Mackenzie Delta region, N.W.T., Canada. Geophysical Research Letters 35, L06502, 5 pp.

Lawler, J. P., S. D. Miller, D. M. Sanzone, J. Ver Hoef, and S. B. Young. 2009. Arctic network vital signs monitoring plan. Natural Resource Report NPS/ARCN/NRR-2009/088. U.S. Department of the Interior, National Park Service, Natural Resource Program Center, Ft. Collins, Colorado.

Osterkamp, T. E. 2005. The recent warming of permafrost in Alaska. Global and Planetary Change 49:187-202.

Swanson, D. K. 2012a. Monitoring of retrogressive thaw slumps in the Arctic Network, 2011: Three-dimensional modeling of landform change. Natural Resource Data Series NPS/ARCN/NRDS—2012/247. National Park Service, Fort Collins, Colorado.

Swanson, D. K. 2012b. Mapping of erosion features related to thaw of permafrost in Noatak National Preserve. Natural Resource Data Series NPS/ARCN/NRDS—2012/248. National Park Service, Fort Collins, Colorado.

Swanson, D. K., and K. Hill. 2010. Monitoring of retrogressive thaw slumps in the Arctic Network, 2010 baseline data: Three-dimensional modeling with small-format aerial photographs. Natural Resource Data Series NPS/ARCN/NRDS—2010/123. National Park Service, Fort Collins, Colorado.

U. S. Army Corps of Engineers. 1950. Investigation of military construction in arctic and subarctic regions 1945-1948. Main report. U. S. Army Corps of Engineers, St. Paul District, St. Paul, MN. Available from http://oai.dtic.mil/oai/oai?verb=getRecord&metadataPrefix=html&identifier=AD0703360 (accessed 18 October 2013).

Wendler, G., L. Chen, and B. Moore. 2012. The first decade of the new century: a cooling trend for most of Alaska. The Open Atmospheric Science Journal 6:111-116.